BMC Medical Imaging

SYSTEMATIC REVIEW

Open Access

Deep learning-based techniques for estimating high-quality full-dose positron emission tomography images from low-dose scans: a systematic review

Negisa Seyyedi[1], Ali Ghafari[2], Navisa Seyyedi[3] and Peyman Sheikhzadeh[4,5*]

Abstract

This systematic review aimed to evaluate the potential of deep learning algorithms for converting low-dose Positron Emission Tomography (PET) images to full-dose PET images in different body regions. A total of 55 articles published between 2017 and 2023 by searching PubMed, Web of Science, Scopus and IEEE databases were included in this review, which utilized various deep learning models, such as generative adversarial networks and UNET, to synthesize high-quality PET images. The studies involved different datasets, image preprocessing techniques, input data types, and loss functions. The evaluation of the generated PET images was conducted using both quantitative and qualitative methods, including physician evaluations and various denoising techniques. The findings of this review suggest that deep learning algorithms have promising potential in generating high-quality PET images from low-dose PET images, which can be useful in clinical practice.

Keywords Deep Learning, Positron Emission Tomography (PET), Denoising Techniques, Low-Dose PET Images

Introduction

Positron Emission Tomography (PET) is a cutting-edge nuclear medicine imaging modality that generates detailed 3D images. It offers valuable semi-quantitative and metabolic insights into a patient's body by employing a range of radiotracers. These include Fluorodeoxyglucose (^{18}F-FDG), which is widely used, as well as Gallium-68 (^{68} Ga) in conjunction with compounds like PSMA and DOTATATE, among others. This technique enables clinicians to visualize and assess various physiological processes at the molecular level, providing essential information for diagnosis, treatment planning, and monitoring of diseases such as cancer. The PET system detects pairs of gamma rays that are emitted indirectly by a radioactive tracer introduced into the body. This tracer is attached to a molecule that can be either non-metabolically or metabolically active. Then, three-dimensional (3D) PET images of distribution of radiopharmaceutical concentration within the human body are reconstructed by computer analysis. Since the introduction of PET imaging scanner in the early 1970s, it has been widely used to diagnose diseases and to analyze metabolic

*Correspondence:
Peyman Sheikhzadeh
sheikhzadeh-p@sina.tums.ac.ir; psh82@yahoo.com
[1] Nursing and Midwifery Care Research Center, Health Management Research Institute, Iran University of Medical Sciences, Tehran, Iran
[2] Research Center for Evidence-Based Medicine, Iranian EBM Centre: A JBI Centre of Excellence, Tabriz University of Medical Sciences, Tabriz, Iran
[3] Department of Health Information Management and Medical Informatics, School of Allied Medical Science, Tehran University of Medical Sciences, Tehran, Iran
[4] Medical Physics and Biomedical Engineering Department, Medical Faculty, Tehran University of Medical Sciences, Tehran, Iran
[5] Department of Nuclear Medicine, Imam Khomeini Hospital Complex, Tehran University of Medical Sciences, Tehran, Iran

processes in the body in various medical fields such as oncology, neurology, cardiology, etc. [1].

In PET imaging, there is a tendency to choose a high injection dose of radionuclide or to increase the scanning time to form high-quality PET images; which poses a high risk of radiation damage to patients and healthcare providers. The risk is more serious for children and patients who undergo multiple PET scans during their treatment. However, given the concern about internal radiation exposure, it is desirable to reduce injected radioactivity, but image quality is compromised as a result of this reduction in radiation dose. It is clear that the quality of a low-dose PET (LD PET) image will be inferior to that of a full-dose PET (FD PET) image due to the factors mentioned that occur during the acquisition process. As a result, the LD PET image will exhibit increased noise and potentially unnecessary artifacts, along with a decreased signal-to-noise ratio (SNR) [2].

A range of methods [3–6] have been proposed to improve the image quality and reduce PET image noise and artifacts, which can be generally classified into two categories: image post-processing [3, 7] and incorporation into iterative reconstruction [5, 6, 8, 9]. Image post-processing methods apply filters or statistical reconstruction algorithms, but they may introduce blurring or distortions. Iterative reconstruction methods incorporate noise reduction techniques into the reconstruction process, such as Penalized Likelihood or Time-of-Flight PET, to improve contrast, resolution, and lesion detectability. Resolution modeling can also improve spatial resolution and reduce noise. The choice of method depends on the scanner, acquisition protocol, and clinical application.

In recent years, deep learning methods have shown an explosive popularity in medical imaging fields to reduce the noise of LD PET images and restore the image quality to the same level as FD PET. These methods have several advantages over traditional image post-processing and iterative reconstruction methods, including higher image quality, shorter processing times, and greater generalizability.

Therefore, this systematic review aims to provide a comprehensive overview of the current state-of-the-art in deep learning-based techniques for estimating FD PET images from LD scans and to identify the challenges and opportunities for future research in this area.

Materials and methods

Literature Search

This study was performed using the Preferred Reporting Items for Systematic Reviews [10]. The study protocol was registered in PROSPERO (CRD42022370329). A systematic search was conducted in different databases including PubMed, IEEE, SCOPUS, Web of Science, databases through July 2023. The search algorithm, which can be found in Table 1, was adapted to include combinations of equivalent terms. Additionally, the reference lists of related articles were scrutinized using the snowball method to identify further relevant articles.

Table 1 A search was conducted in PubMed, Web of Science, Scopus and IEEE databases in July 2023, which yielded 331 articles from PubMed, 342 from Web of Science, 25 from Scopus, and 316 from IEEE

Database	Search string
PubMed	((“low-dose”[tiab] OR “low dose”[tiab] OR (“low”[tiab] AND “dose”[tiab]) OR reconstruction[tiab] OR denoising[tiab] OR “low count”[tiab] OR “reduced dose”[tiab] OR (“reduc*”[tiab] AND “dose” [tiab])) AND (“deep learning” [All Fields] OR “Deep Learning”[MeSH Terms] OR “generative adversarial network*” [All Fields] OR “neural network*” [All Fields] OR “supervised learning” [All Fields] OR “Supervised Machine Learning”[MeSH Terms] OR “machine learning”[All Fields] OR “machine learning”[MeSH] OR “Artificial Intelligence”[tiab]) AND (PET[tiab] OR “Positron Emission Tomography”[tiab] OR “Positron-Emission Tomography”[MeSH Terms]))
Web of Science	(((TS = (low) AND TS = (dose)) OR TS = (“low dose”) OR TS = (low-dose) OR TS = (“low count”) OR TS = (“reduced dose”) OR (TS = (reduc*) AND TS = (dose))) AND (ALL = (“deep learning”) OR ALL = (“neural network*”) OR ALL = OR ALL = (“generative adversarial network*”) OR ALL = (“supervised learning”) OR ALL = (“Supervised Machine Learning”) OR ALL = (“machine learning”)) AND (TS = (“PET”) OR TS = (“Positron Emission Tomography”) OR TS = (“Positron-Emission Tomography”)))
Scopus	((TITLE-ABS(low) AND TITLE-ABS(dose)) OR TITLE-ABS(“low dose”) OR TITLE-ABS(low-dose) OR TITLE-ABS(“low count”) OR TITLE-ABS(“reduced dose”) OR (TITLE-ABS(reduc) AND TITLE-ABS(dose))) AND (ALL(“deep learning”) OR ALL(“neural network”) OR ALL(“generative adversarial network”) OR ALL(“supervised learning ”) OR ALL(“Supervised Machine Learning”) OR ALL(“machine learning”)) AND (TITLE-ABS(“PET”) OR TITLE-ABS(“Positron Emission Tomography”) OR TITLE-ABS(“Positron-Emission Tomography”)) AND ((PUBYEAR < 2023) OR PUBDATETXT(“January 2023” OR “February 2023” OR “March 2023” OR “April 2023” OR “May 2023” OR “June 2023” OR “July 2023”))
IEEE	((“Abstract”:“low-dose” OR “Abstract”:ultra-low* OR “Full Text & Metadata”:ultra low* OR “Full Text & Metadata”:“low dose” OR (“Abstract”:“low” AND “Abstract”:“dose”) OR “Full Text & Metadata”:reconstruction OR “Full Text & Metadata”:denoising OR “Full Text & Metadata”:“low count” OR “Full Text & Metadata”:“reduced dose” OR (“Abstract”:reduc* AND “Abstract”:“dose”)) AND (“Abstract”:“deep learning” OR “Full Text Only”:generative adversarial network* OR “Full Text Only”:neural network* OR “Full Text Only”:“supervised learning” OR “Abstract”:“Supervised Machine Learning” OR “Abstract”:“machine learning” OR “Abstract”:“Artificial Intelligence”) AND (“Abstract”:PET OR “Abstract”:“Positron Emission Tomography” OR “Abstract”:“Positron-Emission Tomography”))

Inclusion and Exclusion

Eligible articles were considered based on the following inclusion criteria:

a) Studies should present the development of at least one DL model for denoising of LD PET images referring to any organs of humans.
b) These comparative studies should include the quality comparison of PET images between images obtained from deep learning models and FFD PET ones.
c) Articles should report original studies and not reviews/meta-analyses/editorial and letters, concern humans and be written in English.

Quality assessment

The quality assessment of the included articles was conducted using the Checklist for Artificial Intelligence in Medical Imaging (CLAIM) [11]. The CLAIM is a 42-item checklist designed to evaluate medical imaging AI studies. For each item, studies were scored on a 2-point scale (0 or 1), and the CLAIM score was calculated by summing up the scores for each study. Notably, all items in the checklist were equally weighted.

Study selection

The study was conducted in collaboration with all authors of this study. For the process of selecting papers two authors of this study evaluated papers. In initial evaluation, first the titles and abstracts of papers were examined. In this stage, papers that are not relevant to the search topic were excluded. Then, a complete review of the full text of the papers was performed, and papers examining the development of deep learning algorithms on reducing the noisy and increasing the quality of images in LD PET imaging were included. Any disagreements in the selection process were discussed with a third member of the research team for consensus.

Data extraction

Subsequently, the key characteristics of the studies were captured, and data was extracted, including: (a) first author and year of publication, (b) number of samples, (c) study design, (d) demographic and clinical characteristics of patients, (e) dose reduction factor, (f) the architecture of proposed deep learning algorithm, (g) data preprocessing steps, (h) evaluation methods and image quality metrics. If more than one algorithm was investigated in one study, we would extract data from the algorithm with the highest performance.

Data and statistical analysis

The data were aggregated and summarized descriptively and synthesized in narrative and tabular forms. The data were tabulated to present general information about the studies including authors, year, paper type, research method, intervention, outcomes.

Results

Search results

The initial systematic search identified 1032 studies. After removing the duplicates, 799 articles were retrieved for title and abstract assessment, and 213 articles were selected for full-text evaluation. 159 articles were excluded if they did not have a proposed architecture, they only compared different architectures, or their dataset was animal. Finally, 56 articles published between 2017 and 2023 were included in this systematic review, two of which were obtained from the reference search of articles by snowballing. The aim of all studies was to demonstrate the potential of LD to FD conversion by deep learning algorithms. The flowchart of selection for included studies is demonstrated in Fig. 1.

Quality assessment

Table 2 presents a summary of the quality assessment for the included studies using the CLAIM tool.

Dataset characteristics

The studies obtained have conducted both prospective and retrospective analyses. Among these, Studies [16, 26–29, 37, 40, 41, 64, 66] were retrospective, while the others were prospective. The analyses involved varying sizes of datasets, with the study by Kaplan et al. having the smallest dataset, consisting of only 2 patients. The majority of the studies analyzed fewer than 40 patients. However, the studies with the most substantial sample sizes were numbers [7, 66] and [54], which included 311 and 587 samples, respectively. (Please refer to Table 3 for further details, and additional information is available in the Supplementary material).

Datasets may be real world data or simulated as in the work of [30, 53, 60], including normal, diseased, or both subjects in different body regions. In this regard, the patients were scanned from the brain [12, 13, 15, 17, 18, 20, 21, 26–29, 31, 39–41, 46, 52, 53, 55, 60, 64, 65, 68], lung [19, 21, 25, 34], bowel [44], thorax [34, 45], breast [50], neck [57], abdomen [63] regions, and twenty two studies were conducted on whole body images [14, 16, 22, 23, 32, 33, 35–38, 42, 43, 48, 49, 51, 54, 58, 59, 61, 62, 66, 67]. PET data is acquired through the use of various scanners and the administration of different radiopharmaceuticals such as ^{18}F-FDG, ^{18}F-florbetaben, ^{68} Ga-PSMA,

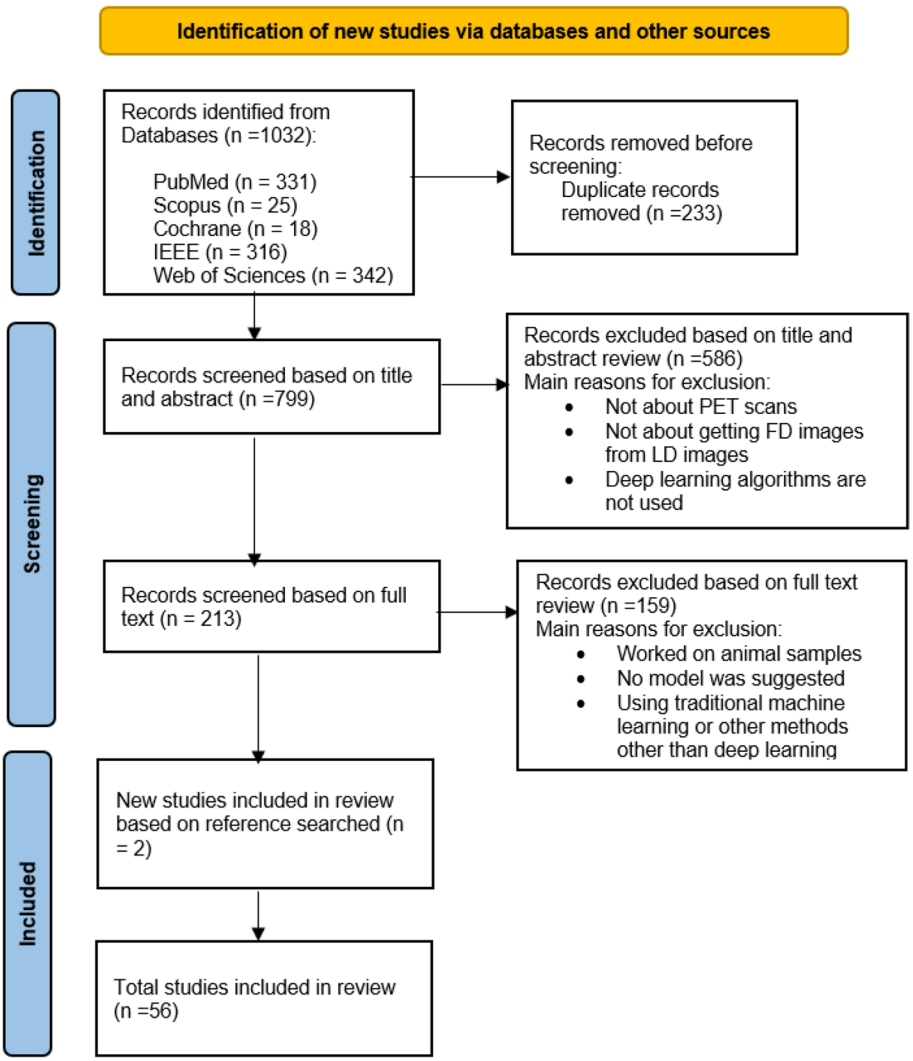

Fig. 1 Flow diagram of study selection

^{18}F-FE-PE2I, ^{11}C-PiB, ^{18}F-FDG, ^{18}F-AV45, ^{18}F-ACBC, ^{18}F-DCFPyL, or amyloid radiopharmaceuticals. These radiopharmaceuticals are injected into the participants at doses ranging from 0.2% up to 50% of the full dose in order to estimate FD PET images.

In these studies, the data are pre-processed in order to prepare them as input to the model, and in some articles, data augmentation has been used to compensate for the lack of sample data [13, 18, 19, 47].

Design

In order to synthesize high-quality PET images using deep learning techniques, it is necessary to train a model to learn mapping between LD and FD PET images.

Several models based on CNN, UNET, generative adversarial network (GAN), have been proposed in various studies, with the GANs being the well-received method among them.

After a systematic literature review for medical imaging reconstruction and synthesis studies, this paper totally included thirteen CNN-based models ([12–14, 21, 27, 31, 36, 42, 43, 51, 56, 58, 67]), fifteen UNET-based models ([17, 19, 22, 26, 28, 37, 39, 40, 44, 45, 48, 55, 61, 62, 66]), twenty one GAN-based models ([15, 16, 18, 20, 23–25, 29, 32, 33, 35, 38, 41, 46, 47, 49, 50, 52–54, 65]), two transformer models ([60, 69]) and some other specialized models ([48, 57, 59–61, 63, 68]) to discuss and reproduce for comparison. The frequency of models employed in the reviewed studies can be seen in Fig. 2.

To the best of our knowledge, Xiang et al. [12] were among the first to propose a CNN- based method in 2017 for FD PET image estimation called auto-context CNN. This approach combines multiple CNN modules

Table 2 The Checklist for Artificial Intelligence in Medical Imaging scores

Author /Publish year	Title/ Abstract Score (n/2)	Introduction Score (n/2)	Methods Score (n/28)	Results Score (n/5)	Discussion Score (n/2)	Other Information Score (n/3)	Total Score (n/42)
Lei Xiang/ 2017 [12]	1	2	19	3	0	1	26
Junshen Xu / 2017 [13]	1	2	18	3	1	0	25
Sydney Kaplan/ 2018 [14]	1	2	17	2	1	0	23
Yan Wang/ 2018 [15]	1	2	18	3	1	0	25
Yang Lei/ 2019 [16]	2	2	21	2	1	1	29
Kevin T. Chen/ 2019 [17]	2	2	22	4	2	1	33
Jiahong Ouyang/ 2019 [18]	2	2	16	2	2	1	25
Wenzhuo Lu/ 2019 [19]	2	2	16	3	2	1	26
Yan Wang/ 2019 [20]	1	2	17	2	2	1	25
Kuang Gong/ 2019 [21]	1	2	19	2	2	1	25
Jianan Cui/ 2019 [22]	2	2	18	4	1	0	27
Yu Gong/ 2020 [23]	1	2	15	2	1	0	21
Kui Zhao / 2020 [24]	1	2	19	2	2	1	27
Long Zhou/ 2020 [25]	1	2	17	2	2	1	25
Amirhossein Sanaat/ 2020 [26]	2	2	18	3	2	1	28
Karl Spuhler/ 2020 [27]	1	2	19	4	1	0	25
Kevin T. Chen/ 2020 [28]	2	2	17	3	2	1	25
Si Young Yie / 2020 [29]	2	2	17	3	1	1	25
Abolfazl Mehranian/ 2020 [30]	2	2	20	4	1	1	30
Qiupeng Feng/ 2020 [31]	1	2	17	2	1	0	21
Yang Lei/ 2020 [32]	1	1	13	2	1	1	19
Amirhossein Sanaat/ 2021 [33]	2	2	23	4	2	1	34
Bo Zhou / 2021 [34]	1	2	20	4	2	1	30
Zhanli Hu/ 2021 [35]	1	2	19	3	2	0	27
Yan-Ran (Joyce) Wang/ 2021 [36]	2	2	21	4	2	1	32
Hui Liu / 2021 [37]	1	2	17	4	1	1	26
Hengzhi Xue / 2021 [38]	1	2	19	2	0	0	25
Kevin T. Chen/ 2021 [39]	1	2	17	4	1	0	25

Table 2 (continued)

Author /Publish year	Title/ Abstract Score (n/2)	Introduction Score (n/2)	Methods Score (n/28)	Results Score (n/5)	Discussion Score (n/2)	Other Information Score (n/3)	Total Score (n/42)
Viswanath P. Sudarshan/ 2021 [40]	0	2	19	4	1	1	26
Song Xue / 2021 [41]	2	2	20	4	2	1	31
Ashok J. Theruvath / 2021 [42]	1	2	15	3	2	0	23
Akshay S. Chaudhari/ 2021 [43]	1	2	15	2	2	0	22
Christian J. Park/ 2021 [44]	1	1	19	2	1	1	25
Claes Nøhr Ladefoged / 2021 [45]	1	2	18	3	1	1	26
Zhao Peng / 2021 [46]	2	2	16	3	2	1	26
Ali Ghafari / 2022 [47]	2	2	18	3	2	1	28
Yan Xing/ 2022 [48]	1	2	19	3	2	1	28
Yang Zhou / 2022 [49]	2	2	19	2	2	0	27
Tomoyuki Fujioka / 2022 [50]	2	2	16	3	2	0	25
Bart M. de Vries/ 2022 [51]	2	2	18	4	2	1	29
Hanyu Sun / 2022 [52]	1	2	17	3	0	0	23
Yanmei Luo/ 2022 [53]	2	2	15	3	1	1	24
René Hosch / 2022 [54]	1	2	19	4	1	0	27
Raphaël Sura Daveau / 2022 [55]	2	2	15	4	2	1	26
Fuquan Deng / 2022 [56]	2	2	18	4	2	1	29
Lipei Zhang / 2022 [57]	2	2	17	4	2	1	28
Taisong Wang / 2022 [58]	1	2	20	4	2	1	30
Takaaki Yoshimura / 2022 [59]	1	2	20	2	1	0	26
Rui Hu / 2022 [60]	2	2	19	3	1	0	27
Bo Zhou / 2023 [61]	1	2	19	3	2	1	28
Jiadong Zhang / 2023 [62]	0	2	20	3	2	1	24
Caiwen Jiang / 2023 [63]	1	2	18	2	1	0	24
Yuya Onishi / 2023 [64]	1	2	17	2	2	1	25
Yu Fu / 2023 [65]	1	2	20	4	1	1	27
Yiyi Hu / 2023 [66]	2	2	21	4	2	1	32
Kun Liu / 2023 [67]	2	2	18	2	1	1	26
Behnoush Sanaei / 2023 [68]	1	2	20	4	2	1	30
Se-In Jang/ 2023 [69]	1	2	16	2	1	1	23

Table 3 characteristics of the included studies

author/ publication date	Anatomic site / disease	Characteristics of datasets			imaging					
		Sample size	Train/Val/Test	Input	scanner	LD PET (Input)	Approach	SD PET (Target)	multi-modal information	Reduction Factor
Lei Xiang/ 2017 [12]	Brain	16 Subjects	$4.5*10^5$–1 patches for training and 1 patch for testing	Concatenation of the two patches of LPET and T1-weighted with two channels	Siemens Biograph mRI PET-MR system	A quarter of the standard dose (acquired in a three-minute short period, with standard-dose tracer injection)	Scan duration/ time reduction	average of 203 MBq of 18FDG, obtained in a 12-min period within one hour of tracer injection	T1- weighted MRI	4X
Junshen Xu / 2017 [13]	glioblastoma	9 Patients	Not mentioned	2.5D multi-slice inputs	PET/MRI TOF-enabled system (SIGNA, GE Healthcare)	randomly selecting 0.5% of the count events, spread uniformly over the entire acquisition period	Random sampling of count events	370 MBq of 18FDG (acquired for about 40 min, beginning 45 min after injection)	-	200X
Sydney Kaplan/ 2018 [14]	Whole body (split into four regions: brain, chest, abdomen, and pelvis)	2 patients	One patient (435 slices or 96,692 patches) for training and one patient (440 slices or 53,360 patches) for testing	Filtered Low dose image patch	Investigational Philips Vereos PET/CT system	1/10th counts	Sampling of count events	Full-dose 18FDG	-	10X
Yan Wang/ 2018 [15]	Brain	16 = 8 normal subjects and 8 subjects diagnosed as MCI	Not mentioned	3D LD PET patches	Siemens Biograph mMR PET-MR scanner	3-min LD PET scans following FD scan	Scan duration/ time reduction	an average of 203 MBq (corresponding to an effective dose of 3.86 mSv) of 18FDG with 12 min of scanning	-	4X
Yang Lei/ 2019 [16]	whole-body FDG oncology patient	25 patients	25 patients for training	LD PET patches	Discovery 690 PET/CT scanner (General Electric)	Low count PET data were created by histogramming the emission data to 1/8 the bed duration for all bed positions	Sampling of count events	370 MBq (BMI < 30) or 444 MBq (BMI ≥ 30) of 18FDG followed by a 60-min uptake period	-	8X
Kevin T. Chen/ 2019 [17]	Brain	40 datasets from 39 patients	32 datasets for training and 8 ones for testing	the multicontrast MR images and the single slice LD PET	An integrated PET/ MRI scanner with time-of-flight capabilities (SIGNA PET/ MR, GE Healthcare)	1/100th of the events	Random sampling of count events	An intravenous injection of 330 MBq ± 30 of the amyloid radiotracer 18F-florbetaben (Piramal Imaging) and PET data were acquired 90–110 min after injection	T1-weighted, T2-weighted, and T2 fluid-attenuated inversion recovery morphologic MR images were acquired,	100X
Jiahong Ouyang/ 2019 [18]	Brain/ AD patients	40 PET datasets from 39 participants	Not mentioned	Multi-slice inputs, stack of nine neighboring slices from the LD PET images	simultaneous PET/MRI (Signa, GE Healthcare	randomly undersampling of raw list-mode PET data by a factor of 100 to reconstruct 1% LD PET scans	Random sampling of count events	injection of 330 ± 30 MBq of the amyloid radiotracer 18F-florbetaben	2-point Dixon MR Atlas	100X

Table 3 (continued)

author/ publication date	Anatomic site / disease	Characteristics of datasets			imaging					
		Sample size	Train/Val/Test	Input	scanner	LD PET (Input)	Approach	SD PET (Target)	multi-modal information	Reduction Factor
Wenzhuo Lu/ 2019 [19]	Lung nodules	10 patients	Not mentioned	Fully 3D LD PET patch	Siemens Biograph mCT PET/CT scanner	10% LD data was generated by uniform down-sampling of the list-mode data during these 20 min	Uniform down-sampling of the list-mode data	10 mCi FDG injection and list mode data was generated between 60 and 80 min post-injection	-	10X
Yan Wang/ 2019 [20]	Brain	16 = 8 normal subjects and 8 subjects diagnosed as MCI	Not mentioned	Large 3D image patches consist of an LD PET, a T1-MRI, an FA-DTI and an MD-DTI	PET acquisition data were simulated to model the acquisition geometry of the Siemens Biograph mMR system	25% of the normal count level	Count reduction	Not mentioned	T1-MRI and DTI includeFA, MD, RD	4X
Kuang Gong/ 2019 [21]	Brain and lung	3 dynamic brain PET scans for the brain-imaging network and 6 patients datasets for the lung-imaging network	520 training pairs	LD PET image patches	Simulated mCT time-of-flight PET/CT scanner	Images from 1/5th of the counts	Down-sampling count events	For brain-imaging: brain PET scans of 70 min with 5 mCi FDG injection for lung-imaging:1-h FDG dynamic scan with 5 mCi injection) acquired on a GE 690 scanner	-	5X
Jianan Cui/ 2019 [22]	Whole-body	30 patients for the PET/MR dataset	Not mentioned	MR prior image	Simulated Siemens mCT scanner	Not mentioned	Not mentioned	The sinogram data was generated from the last 5 min frame of a one-hour 18F-FDG scan with 1 mCi dose injection	T1-weighted MR image as prior	Not mentioned
Yu Gong/ 2020 [23]	Torso	Nine patients	7 patients for training and 2 patients for testing	3D LD PET	Neusoft NeuWise EWN ToF PET/CT scanner	LD PET images from the 20% uniform under-sampled LD PET scans	Under-sampling	The patients were injected with fluorodeoxyglucose (F-18) in 0.15 mCi/kg and scanned 90–110 min after injection	-	5X
Kui Zhao / 2020 [24]	Brain	109 clinic patient	89 patients for training. 10 patients for validation and 10 patients for testing	LD PET patches	Minfound Scint-Care PET/CT 720L scanner	30% counts of original scan	Random discard of events	Scans were taken about 5 min (45–60 min after injection) with injection of 370.81 ± 64.38 MBq of 18F-FDG	-	3.3X
Long Zhou/ 2020 [25]	Lung	18 patients	14 patients for training and 4 for testing	Patches of LD input image	Siemens Biograph mCT scanner	Randomly discarding events in the PET list-mode data towards the predefined true count level of 1 × 106	Random discard of events	uptake period of 60 min with injection of 218.3 ± 5.18 MBq of 2-deoxy-2-(18F) FDG	-	Not mentioned

Table 3 (continued)

author/ publication date	Anatomic site / disease	Characteristics of datasets			imaging					
		Sample size	Train/Val/Test	Input	scanner	LD PET (Input)	Approach	SD PET (Target)	multi-modal information	Reduction Factor
Amirhossein Sanaat/ 2020 [26]	Neurodegenerative disease	140 patients	100 patients for training, 20 for validation and 20 for training	LD PET images and sinograms	A Biograph mCT scanner (Siemens Healthcare)	Five percent of the events were randomly selected from the FD list-mode PET data to simulate a realistic LD acquisition	Randon extraction of data	A 20-min brain PET/CT scan after injection of 205 ± 10 MBq of 18F-FDG	-	20X
Karl Spuhler/ 2020 [27]	Brain	35 PET studies	Training (n = 30) and testing (n = 5)	2D slices of low-count PET images	A Siemens Biograph mMR PET/MRI scanner	Low-count PET data were generated through Poisson thinning. Specifically, low-count PET data with a dose reduction factor 90% (one-tenth of original counts) were generated	Poisson thinning	Each subject was administered between 148–185 MBq (4-5 mCi) of 18F-FDG	-	10X
Kevin T. Chen/ 2020 [28]	Brain/Alzheimer's disease	80 PET/MRI studies, split equally between two sites (Site 1 and 2)	Not mentioned	Not mentioned	Site 1: Signa PET/MRI, GE Healthcare; Site 2: mMR, Siemens Healthineers,	Ultra-low-count data obtained from under-sampling by a factor of 100 (Site 1) or the first minute of PET acquisition (Site 2)	Under-sampling	20 min of list-mode PET data (90–110 min post-injection) were reconstructed as ground-truth (330 ± 30 MBq of the amyloid radiotracer [18F] florbetaben)	T1-weighted, T2-weighted, and T2 FLAIR morphological MR images were acquired	20X & 100X
Si Young Yie / 2020 [29]	Brain	14 patients	10 for training and 4 for testing	Image patches (2D)	A Biograph mCT40 scanner	We also generated 40-s-long data by adding four non-overlapping 10-s bins	Not mentioned	The list-mode PET data were acquired 60 min after the intravenous injection of 18F-FDG (5.18 MBq/kg) for 5 min in a single bed position. From the list-mode data, we generated a total of 100 data bins with 10-s duration.(300-s-long reference data by adding all list-mode data.)	-	7.5X
Abolfazl Mehranian/ 2020 [30]	Brain	210 Simulation datasets and 45 PET-MR brain in-vivo datasets	35 training and ten test datasets	LD sinogram (3D)	A Siemens mMR scanner	For LD sinograms randomly chosen count levels in [90–120] million with PSF of 4.5-mm FWHM were considered	Not mentioned	For HD sinograms, 1 billion counts and a PSF with 2.5-mm full-width-at-half-maximum (FWHM) Gaussian kernels were considered	T1-weighted MPRAGE MR images	Not mentioned
Qiupeng Feng/ 2020 [31]	Brain	Nine patients	6 patients for training, 2 patients for validation and 1 for testing	LD sinogram	Not mentioned	Randomly generated 1/500th LD sinograms with 0.2% down-sampling of count events	Down-sampling of count events	Standard dose of 18F-2-deoxyglucose (18FDG, 370 MBq)	-	500X

Table 3 (continued)

author/ publication date	Anatomic site / disease	Characteristics of datasets			imaging					
		Sample size	Train/Val/Test	Input	scanner	LD PET (Input)	Approach	SD PET (Target)	multi-modal information	Reduction Factor
Yang Lei/ 2020 [32]	Whole body	16 patients	Not mentioned	3D patch fashion from low count PET and CT images	Not mentioned	Low count PET data were created by histogramming the emission data to one-eighth the bed duration for all bed positions	histogramming	acquired by a 60-min uptake period. Emission data were collected based on BMI for 1.5–2.5 min for each bed position	CT	8X
Amirhossein Sanaat/ 2021 [33]	Whole body	100 patients (Fifteen studies were excluded)	60 patients for training, 10 for validation and 15 for testing	LD PET images	Biograph mCT PET/CT scanner	Separate fast PET acquisition corresponding to ~ 1/8th the FD scan duration prior to FD PET acquisition (120 kVp, 80 mAs)	Scan duration reduction	60 min post-injection of 240 ± 50 MBq of 18F-FDG	-	8X
Bo Zhou / 2021 [34]	Thorax	28 pancreas 18F-FPDTBZ PET/CT studies (15 healthy patients and 13 Type-2 diabetic patients)	Not mentioned	A set of LD gated PET images	A 4- ring Siemens Biograph mCT scanners	LD images were reconstructed with 1.5% of the (high-dose) list-mode data with uniform sampling Thus, each LD gated image was reconstructed with about 0.25% of the list-mode data	Uniform Sampling	FD gated image was reconstructed with about 16.67% of the list-mode data acquired from 18F-FPDTBZ PET/CT studies with average administered dose of 9.13–1.37 mCi	-	66.67X
Zhanli Hu/ 2021 [35]	Full-body scans of 16 males and 14 females	30 patients	80% of the images were used for training, and 20% of the images were used for testing	2D sinogram data	GE Discovery PET/CT 690 machine	Patient PET images were forward-projected to generate a noise-free sinogram. Then, a uniform background of 20% total true coincidences was added to simulate random and scatter events	Not mentioned	Not mentioned	-	Not mentioned
Yan-Ran (Joyce) Wang/ 2021 [36]	Whole-body	33 children and young adults/ malignant lymphoma	23 patients for training and 10 for validation and testing	Axial simulated ultra-LD 18F-FDG PET images and simultaneously acquired axial contrast-enhanced T1-weighted MRI image	A 3 T Signa PET/MRI scanner	6.25% (0.18 mBq/kg) LD 18F-FDG PET images were simulated by unlisting the PET list-mode data and reconstructing them based on the percentage of used counts	Unlisting the PET list-mode	1 h after intravenous injection of 18F-FDG at a dose of 3 MBq/kg	T1-weighted MRI	16X

Table 3 (continued)

author/ publication date	Anatomic site / disease	Characteristics of datasets			imaging					
		Sample size	Train/Val/Test	Input	scanner	LD PET (Input)	Approach	SD PET (Target)	multi-modal information	Reduction Factor
Hui Liu / 2021 [37]	Whole body	100 subjects	Not mentioned	Fully 3D patches of low-count PET images	A Siemens Biograph mCT	40% count level	Independent uniform down sampling	The subjects were injected with 18F-FDG and a whole-body protocol with continue-bed-motion scanning was used	-	2.5X
Hengzhi Xue / 2021 [38]	Whole-body scan	30 patients	24 patients as the training set and data from 6 patients as the test set	Low Count PET sinogram data	GE Discovery PET/CT 690 machine	Normalization of the simulated sinogram data to 5 M, 500 K, and 50 K counts to represent different dose. Also, independent Poisson noise was introduced 20 times in the sinogram data to simulate real noise data	Not mentioned	Not mentioned	-	Not mentioned
Kevin T. Chen/ 2021 [39]	Brain	32 participants for pre-trained network with 18 new participants	Not mentioned	MR, Actual and sampled LD images	SIGNA PET/MR (GE Healthcare)	6.64 ± 3.57 MBq 18F-florbetaben injection (2.2 ± 1.3% of standard)	Ultra-low-dose injection	300 ± 14 MBq 18F-florbetaben injection	The T1-, T2-, and T2 FLAIR–weighted MR images were acquired simultaneously with PET on the same scanner	50X
Viswanath P. Sudarshan/ 2021 [40]	Brain	28 healthy individuals	Randomly selected 20 subjects for training, 2 subjects for validation, and the remaining for testing	Multimodal 2.5D (the LD PET image and the multicontrast MRI images) For each subject, we obtained 100	A 3 T Siemens Biograph mMR system	To simulate the LD-PET data, we randomly selected around 3.4 × 106 counts, spread uniformly over the scan duration, resulting in a DRF of around 180×	Uniform random sampling	The SD-PET image was reconstructed using counts obtained over a duration of 30 min, starting 55 min after the administration of the tracer (230 MBq F-18-FDG)	The MRI contrast images, i.e., ultra-short echo time (UTE), T1 MPRAGE, and T2-SPC, were acquired during the PET scan	180X

Table 3 (continued)

author/ publication date	Anatomic site / disease	Characteristics of datasets			imaging					
		Sample size	Train/Val/Test	Input	scanner	LD PET (Input)	Approach	SD PET (Target)	multi-modal information	Reduction Factor
Song Xue / 2021 [41]	Brain	310 subjects	237 patients for training and 63 for testing	LD PET scans from different scanners and tracers (3D)	The subjects were scanned on 3 different PET scanners (GE Discovery MI, Siemens Biograph mCT, Siemens Biograph Vision)	Each simulated LD PET with a certain DRF was reconstructed from the counts of a time window resampled at the middle of the acquisition with correspondingly reduced time. (The model was trained by mixing the image pairs of all DRF up to 20 from GE, Discovery MI, and later tested on datasets from different scanners and tracers with DRF up to 100.)	Not mentioned	Not mentioned	-	Up to 20X / 100X
Ashok J. Theruvath / 2021 [42]	Whole body/ lymphoma	20 patients	Not mentioned	2.5D LD images	A 3-T Signa PET/MRI scanner	LD PET images were retrospectively simulated by unlisting the PET list-mode data and reconstructing them based on the percentage of coincidence events	Unlisting PET list-mode data	18F-FDG was administered intravenously approximately 60 min before scanning at a dose of 3 MBq per kilogram of body weight (3-min 30-s acquisitions per PET bed)	Gradient-echo fat-saturated T1-weighted	2X
Akshay S. Chaudhari/ 2021 [43]	whole-body cancer	50 subjects from three separate hospitals	Not mentioned	2.5D LD PET	Not mentioned	Fourfold low-count PET	Not mentioned	A mean FDG dose of 12.0 ± 1.9 mCi were evaluated	-	4X
Christian J. Park/ 2021 [44]	Bowel/ Crohn disease	20 subjects	Not mentioned	Combinations of LD PET images and the MR Dixon water-only images adjacent slices were used as pseudochannels (2.5D)	A simultaneous PET/MR scanner (Signa PET/MR, GE Healthcare, Waukesha, WI)	using 20% of PET counts	Using counts from first 20% scan acquisition duration	Approximately 60 min after intravenous injection of 185 MBq (± 10%) of FDG, subjects were scanned (5 min per bed)	Non-contrast and free-breathing two-point Dixon MR images	5X

Table 3 (continued)

author/ publication date	Anatomic site / disease	Characteristics of datasets			imaging					
		Sample size	Train/Val/Test	Input	scanner	LD PET (Input)	Approach	SD PET (Target)	multi-modal information	Reduction Factor
Claes Nøhr Ladefoged / 2021 [45]	thorax region/ chronic ischemic heart disease	168 patients	Not mentioned	Using the entire LD PET and CT volume	Siemens Biograph mCT/ PET 128-slice scanner	Simulating a reduced dose by keeping counts at thresholds 1% and 10%, corresponding to 3 MBq and 30 MBq, respectively, on average, using LMChopper	Count sampling	300 MBq of [18F]FDG (range: 282–404 MBq) was given intravenously and at 60 min post injection (range: 48–105 min)	CT	10X / 100X
Zhao Peng / 2021 [46]	Alzheimer's Disease	25 patients	Not mentioned	multiple adjacent axial slices of the shortened-scanning-time PET images were used as the inputs	Not mentioned	Shortened-scanning-time reconstruction (5-min)	Scan time reduction	Normal-scanning-time (20-min from the 50th to 70th minute) injected with 370 ± 37 MBq 18F-AV45 radiopharmaceutical	-	4X
Ali Ghafari / 2022 [47]	Whole-body	42 patients (41 18F-FDG and one 68 Ga-PSMA)	From 41 18F-FDG PET images one patient was randomly selected and set aside as the internal validation,	2D slices	A 5-ring BGO-based PET/CT scanner (GE discovery-IQ)	1/8th scan duration	Scan duration reduction	18F-FDG scan with a standard radioactivity dose of 294.52 ± 45.18 MBq	-	8X
Yan Xing/ 2022 [48]	Whole-body	52 oncological patients	Not mentioned	LD image patches	Digital PET/CT scanner (uMI 780, United Imaging Healthcare, China)	50% of the total counts	Rebinning the list-mode data	The injected dose was 3.1–4.3 MBq/kg, while the acquisition time was 90–180 s/bed for the body part	-	2X
Yang Zhou / 2022 [49]	Full-body	105 patients	Not mentioned	3D low-dose PET image	PoleStar m660 PET/CT system	The LD raw data is synthesized by randomly selecting 1/6 of the raw count list-mode datasets	Random Selection of counts	Injection dose of around 0.1 mCi/kg of 18F-fluorodeoxyglucose (FDG)	-	6X
Tomoyuki Fujioka / 2022 [50]	Breast	49 breasts images from 45 patients	Patients were randomly assigned to a training image set ($n=16$), validation image set ($n=7$), and test image set ($n=26$)	LD PET transverse slices (2D)	Elmammo dbPET scanner (Shimadzu, Kyoto, Japan)	PET images with short acquisition times were reconstructed from 420 s full-time data divided into 26 s (6.25%), 52 s (12.5%), 105 s (25%), and 210 s (50%) from the start of acquisition	Dividing full-time data	PET scanning was performed for 7 min for each breast in the prone position approximately 90 min after receiving 18F-FDG (3 MBq/kg) injection	-	2X / 4X / 8X / 16X

Table 3 (continued)

author/ publication date	Anatomic site / disease	Characteristics of datasets			imaging					
		Sample size	Train/Val/Test	Input	scanner	LD PET (Input)	Approach	SD PET (Target)	multi-modal information	Reduction Factor
Bart M. de Vries 2022 [51]	whole-body/ patients with stage I–IV non-small-cell lung carcinoma	60 patients (40 from center1 and 20 from center 2)	PET data from center1: training ($n=32$), validation ($n=8$). Two CNN models with 18F-FDG and 89Zr-rituximab data from center2: training ($n=8$), validation ($n=2$), independent test ($n=15$)	3D LD PET images	Gemini Big Bore TF PET/CT scanner (Whole-body 18F-FDG PET in LPC)—Ingenuity TF PET/CT and Vereos Digital PET/CT scanners (Whole-body 18F-FDG PET in Amsterdam UMC)—Ingenuity TF PET/CT (89Zr-rituximab PET scans)	Amsterdam UMC 18F-FDG PET data were reconstructed with a 10 s (super-low-count (SLC), 92% scan time reduction), 30 s (low-count (LC), 75% scan time reduction) and 2 min (full-count (FC)) scan duration per bed-position	Scan time Reduction	For 18F-FDG PET scans, 60 min after 259.4 ± 43.8 MBq tracer injection, a 20 min static whole-body 18F-FDG PET scan was acquired (2 min per bed position) Six days after the injection of 73.7 ± 0.3 MBq 89Zr-rituximab, a 60 min static whole-body PET scan (5 min per bed position)	LD CT	4X / 12X
Hanyu Sun / 2022 [52]	Head	67 patients	Not mentioned	Axial head slices of LD PET and T1-weighted MRI	An integrated 3.0 T uPMR 790 PET/MR scanner	LD PET images were created by constructing the histogram of the emission data to 5% (30 s) of the bed duration	Histograming	Samples were acquired from patients 70.6 ± 8.5 min after injection of 18F-fluoro-deoxyglucose (FDG) (224.4 ± 49.9 MBq)	T1-weighted MRI	20X
Yanmei Luo 2022 [53]	Normal control subjects and subjects with mild cognitive impairment	20 phantom dataset and 16 subjects for clinical dataset	2D slices	Not mentioned	A Siemens Biograph mMR PET-MR system	The LD PET scans were simulated by shortening the acquisition time (3 min) at the standard dose (approximately one-quarter of the standard activity (51 MBq) and 0.97 mSv effective dose)	Acquisition time reduction	the standard activity of 18F-flurodeoxyglucose ([18F] FDG) with an average of 203 MBq and an effective dose of 3.86 mSv (SPET scans were conducted for 12 min within 60 min of injection)	-	4X
René Hosch / 2022 [54]	Whole-body	587 patients	387 datasets as training and 200 as test cohort	Six-channel image of PET 2.5d and CT 2.5d images combining (axial slices)	A Biograph Vision 600 PET/CT System	reduced acquisition time PET data were acquired in continuous bed motion mode using a table speed velocity of 50 mm/s	Acquisition time reduction by increasing table speed velocity	Normal acquisition time data were acquired using a table speed velocity of 1.5 mm/s with an emphasis of the abdominal region by a reduced table speed velocity of 0.8 mm/s (The mean ± SD applied activity was 327.8 ± 76.7 MBq of 18F-FDG)	A CT scan in FD or LD technique according to the clinical routine protocol	33.33X

Table 3 (continued)

author/ publication date	Anatomic site / disease	Characteristics of datasets			imaging					
		Sample size	Train/Val/Test	Input	scanner	LD PET (Input)	Approach	SD PET (Target)	multi-modal information	Reduction Factor
Raphaël Sura Daveau / 2022 [55]	Brain	162 patients For [11C]PiB And 509 patients for [18F] FE-PE2I	The data for each cohort were split into train and validation. The [11C] PiB cohort used about 130 patients and the [18F]FE-PE2I cohort used about 407 patients for training	2 mm post reconstruction smoothed low-activity PET	A Biograph Vision PET/CT system (Siemens Healthineers, Erlangen, Germany for [11C] PiB and a Biograph mCT PET/CT (Siemens Healthineers, Erlangen, Germany) for [18F] FE-PE2I	The simulating short scan time by sampling the center 5% of the acquisition, i.e., 1 min for [11C] PiB and 30 s for [18F] FE-PE2I	Randomly sampling 5% of the events	For [11C]PiB a 20 min scan was commenced 40 min after tracer administration (mean activity: 320 ± 79 MBq, range: 150–485 MBq), while for [18F] FE-PE2I a 10 min scan was commenced 30 min after tracer administration (mean activity: 204 ± 12 MBq, range: 180– 255 MBq)	-	20X
Fuquan Deng / 2022 [56]	Prostate cancer	68 Ga-PSMA PET/MRI data of 41 patients	90% of the data set used for training and the remaining 10% used for validation2	A 2D LD PET image and MRI image	uPMR 790 PET/MRI scanner (United Imaging Healthcare)	50% dose PET images	Reducing reconstruction time	Sixty minutes after the patient had been injected with 68 Ga-PSMA (in the range of 111–185 × 106 MBq), scanning data were collected from the PET/MRI scanner	T1-weighted MRI images	2X
Lipei Zhang / 2022 [57]	Neck	70 patients	Not mentioned	Low-count PET with MRI in pixel to pixel shape	An integrated 3.0 T uPMR790 PET/MR scanner (United Imaging Healthcare, Shanghai, China)	Low-count PET data of the neck region using acquisition times such as 10% (2 min), 5% (1) min and 2.5% (0.5) min of the bed duration for all bed positions	Acquisition time reduction	After fasting for at least 6 h, FDG was administered intravenously. PET/MRI data were obtained after 70.6 ± 8.5 min of 224.4 ± 49.9 MBq 18F – FDG	An integrated radiofrequency coil, which used a 3D T1-weighted spoiled gradient-echo sequence with Dixon-based water-fat separation imaging (WFI), was applied in MRI	10X / 20X / 40X

Table 3 (continued)

author/ publication date	Anatomic site / disease	Characteristics of datasets			imaging					
		Sample size	Train/Val/Test	Input	scanner	LD PET (Input)	Approach	SD PET (Target)	multi-modal information	Reduction Factor
Taisong Wang / 2022 [58]	Total-body	26 and 41 oncological patients in Retrospective and Prospective study, respectively	Not mentioned	Not mentioned	A digital uMI 780 PET/CT scanner (United Imaging Healthcare)	The retrospective study simulates the LD scenarios by rebinning the list-mode data into short-duration scans (1/2, 1/3, and 1/4 of the original time), and the prospective study uses real-world LD data with reduced activity injection(1/3 of the standard activity)	Scan Duration Reduction using rebinning	A weight-based 18F FDG (full and one-third) dose was administered to the patient of the two cohorts that allows an accurate dose administration. During an uptake period of about 60 min, the patients were hydrated orally with 0.5–1.0 L of water	CT	2X / 3X / 4X
Takaaki Yoshimura / 2022 [59]	Whole-body	108 patients	Not mentioned	One channel of grayscale LD PET input	Vereos PET-CT system	short-acquisition-time PET images (50%) were reconstructed from identical PET emission data for each patient	Acquisition time reduction	All patients fasted for ≥ 6 h before FDG injection (ca. 4 MBq/kg), and emission scanning was initiated approximately 60-min post-injection	-	2X
Rui Hu / 2022 [60]	Brain	Twenty 3D brain phantoms from BrainWeb	The model has trained with 17 brain samples, and 2 brain samples for testing and 1 brain sample for validation	For each phantom, 10 noncontinuous slices were selected from each of the three orthogonal views	Simulated Siemens Biograph mMR	Low count sinograms (counts)	Count reduction	High count sinograms (counts)	-	10X
Bo Zhou / 2023 [61]	whole-body protocol	175 subjects	120 for training and 55 for validation	2.5 D LD PET images (five continuous axial slices)	Siemens Biograph mCT PET/CT system	uniform down-sampling of the patient list-mode data with down-sampling ratios of 20%, 40%, and 60% for the three groups	Uniform down sampling	Not mentioned	-	1.67X / 2.5X / 5X
Jiadong Zhang / 2023 [62]	Total-body	65 PET images	Not mentioned	LD PET and CT images as inputs for the global total-body network and the inputs to the local network are the four channel images	uEXPLORE PET/CT system	The generating LD sinograms randomly with down-sampling of normal count events	Random down sampling	Not mentioned	CT	Not mentioned

Table 3 (continued)

author/ publication date	Anatomic site / disease	Characteristics of datasets			imaging					
		Sample size	Train/Val/Test	Input	scanner	LD PET (Input)	Approach	SD PET (Target)	multi-modal information	Reduction Factor
Caiwen Jiang / 2023 [63]	Chest-abdomen	50 unpaired SD PET images and 20 paired LD PET and SD PET images for fine-tuning	10 LD PET images (from paired images) for training the E1 and D1, 60 FD PET images for training the E2 and D2. the rest 10 paired images for testing	LD PET and SD PET patches	uEXPLORER PET/CT scanner	Corresponding 1/10th LD PET image were simultaneously reconstructed by 120 s data uniformly sampled from 1200 s data	Uniform sampling	Paired LD and SD PET images were collected by list mode of the scanner with 256 MBq of [18F]-FDG injection and SPET images were reconstructed using 1200 s data between 60 and 80 min after injection	-	10X
Yuya Onishi / 2023 [64]	Brain	18F-AV-45 data from 24 subjects were used for self-supervised pre-training	DIP-based PET image denoising was evaluated using 18F-AV-45, 11C-PIB, and 18F-FDG data from every 10 subjects and also independent 16 noisy samples from 15O-CO2 data	3D patches	The Open Access Series of Imaging Studies (OASIS-3), a public dataset For 18F-AV-45, 11C-PIB and 18F-FDG, Siemens Biograph mMR, Siemens Biograph 40, and Siemens ECAT HR + 962 scanners were used respectively	Ultra-LD PET image was obtained by randomly down-sampling to 1/128th of the list-mode data	Random down sampling	For the 18F-AV-45 scan, the participants received an intravenous bolus of approximately 10 mCi, and a dynamic 70 min emission scan was performed using a Siemens Biograph mMR Participants using 11C-PIB and 18F-FDG received 6 mCi to 20 mCi and approximately 5 mCi, respectively, followed by a dynamic 60 min emission scan	The corresponding T1-weighted MR images acquired individually were interpolated and registered using the normalized mutual information criteria of the SPM tool	128X
Yu Fu / 2023 [65]	Brain	45 subjects with pediatric epilepsy from a local dataset (UMIC dataset)	Not mentioned	LD slices	LDCT and UMIC datasets	5% dose	Not mentioned	LD and FD CT images (LDCT) LD (5%) and FD brain 18F-fluorodeoxyglucose (FDG) PET scans (UMIC dataset)	-	20X
Yiyi Hu / 2023 [66]	Scanning was performed from the base of the skull to the middle of the femur	311 tumor patients	218 patients used for training and 93 for testing	3D LD PET	Discovery MI PET/ CT apparatus (GE Healthcare, USA)	LD imaging was selected for the first 15 and 30 s of each bed collection which were denoted as 8%PET and 17%PET, respectively	Acquisition time reduction	They were intravenously injected with 18F-FDG 3.7 MBq/kg (in list mode, 3 min/bed, 5–7 beds)	CT parameters: tube voltage 120 kV, tube current 60–150 mA, noise index 18, pitch 0.984:1, slice thickness 2.75 mm, rotation time 0.5 s	5.89X / 12.5X

Table 3 (continued)

author/ publication date	Anatomic site / disease	Characteristics of datasets			imaging					
		Sample size	Train/Val/Test	Input	scanner	LD PET (Input)	Approach	SD PET (Target)	multi-modal information	Reduction Factor
Kun Liu / 2023 [67]	Whole-body	37 human bodies provided by Beijing Arrays Medical Imaging Corporation (AMIC)	data were randomly divided into 26 cases as the training set, and 11 cases as the test set	2D radial slice data	Not mentioned	The PET raw data is randomly sampled to reduce the dose to simulate the LD tracer injection in a clinical scenario down-sample the 1/2 and 1/4 dose PET images via Bicubic kernel with scale factor r = 2	Random sampling	Not mentioned	-	2X / 4X
Behnoush Sanaei / 2023 [68]	Head region	140 patients with head and neck malignant lesions	Not mentioned	3-input channels getting 4%, 3%, and 2% as 2D input	A Biograph-6 scanner	The PET raw data was registered in list-mode format, and then 6% LD PET data were extracted from the standard data. Then, lower-dose PET data, including 4%, 3%, and 2%, were generated from the 6% LD data	Sampling raw data	PET images were acquired for an acquisition time of 20 min, about 40 min after the injection	-	25X / 33.34X / 50X
Se-In Jang/ 2023 [69]	whole-body	112 datasets	30 18F-FDG and 30 18F-ACBC for training,4 18F-FDG for validation, and 10 18F-FDG, 10 18F-ACBC, 10 18F-DCFPyL, and 18 68 Ga-DOTATATE for testing	non-overlapping patches of the LD PET image 3d	GE DMI PET/CT scanner	To generate the LD data, 1/4 of the events were extracted from the listmode data	Not mentioned	Not mentioned	-	4X

Table 3 (continued)

author/ publication date	Preprocessing data	DL method/ configuration					Platform	qualitative evaluations	Image quality metrics (quantitative analysis/ clinical metrics)	CLAIM results (percentage)
		model	loss function	optimizer	Training techniques	Evaluation method				
Lei Xiang/ 2017 [12]	Yes	CNN	MSE	SGD	Using auto context strategy, applying batch normalization for every convolution layer	leave-one-out cross-validation strategy	CAFFE	No	PSNR NMSE	61.9%
Junshen Xu / 2017 [13]	Yes	CNN based on an encoder-decoder structure	L1 loss	RMSprop	Residual learning, Batch normalization,	leave-one-out cross validation (LOOCV)	TensorFlow	No	NRMSE PSNR SSIM	59.5%
Sydney Kaplan/ 2018 [14]	Yes	CNN	a loss function combines specific features, namely the gradient and total variation, with the MSE and an adversarial network	ADAM	Residual learning	Not mentioned	Not mentioned	No	RMSE MSSIM PSNR	54.7%
Yan Wang/ 2018 [15]	Yes	Concatenated Conditional GAN	L1 norm	mini-batch SGD	Not mentioned	Leave One-Subject-Out	PyTorch	No	PSNR NMSE SUV	59.5%
Yang Lei/ 2019 [16]	Yes	Cycle-GAN	Cycle-consistent adversarial loss	Adam gradient descent	Using batch normalization in 8 out of 9 layers in the discriminator architecture	hold-out validation with 10 additional patients as test data for model evaluation	python 3.6 and Tensorflow	No	ME PSNR NMSE NCC	69%
Kevin T. Chen/ 2019 [17]	Yes	UNET	L1 norm	Adaptive moment estimation	Training through residual learning	Fivefold cross-validation	Not mentioned	No	RMSE SSIM PSNR	78.5%
Jiahong Ouyang/ 2019 [18]	Yes	GAN	An optimization loss consists of three part: L1 loss, feature matching adversarial loss, task-specific perceptual loss	Adam optimizer	Not mentioned	Fourfold cross-validation	Not mentioned	No	PSNR SSIM RMSE	59.5%

Table 3 (continued)

author/ publication date	Preprocessing data	DL method/ configuration					Platform	qualitative evaluations	Image quality metrics (quantitative analysis/ clinical metrics)	CLAIM results (percentage)
		model	loss function	optimizer	Training techniques	Evaluation method				
Wenzhuo Lu/ 2019 [19]	Yes	Residual UNET	L2 norm	Adam	Using residual learning, and patch-based training	"leave-one-out" fivefold cross-validation	Not mentioned	No	NMSE SNR SUV bias	61.9%
Yan Wang/ 2019 [20]	Yes	Auto-context-based multi-modality GAN	L1 loss	Adam solver with mini-batch SGD	Not mentioned	"Leave-One-Subject-Out" strategy	PyTorch	No	PSNR SSIM	59.5%
Kuang Gong/ 2019 [21]	Yes	CNN	Perceptual loss	Adam optimizer	Not mentioned	Not mentioned	TensorFlow 1.4	No	CRC STD	59.5%
Jianan Cui/ 2019 [22]	Not mentioned	UNET	L2 norm	L-BFGS	Unsupervised deep learning	Not mentioned	Not mentioned	No	CNR	64.2%
Yu Gong/ 2020 [23]	Not mentioned	Westerian GAN	Three loss functions, including the MSE loss, adversarial loss	Adam optimizer	Transfer strategy , Task-specific initialization based on transfer learning	Not mentioned	Python 3.6 with TensorFlow 1.4	No	NRMSE PSNR RFSIM VIF	50%
Kui Zhao / 2020 [24]	Yes	Cycle Westerian GAN	The network combines four types of loss functions: adversarial loss, cycle-consistency loss, identity loss and supervised learning loss	Adam optimizer	Not mentioned	External evaluation with 45 simulated data	Keras with Tensorflow backend	No	NRMSE SSIM PSNR LPIPS SUVmax SUVmean	64.2%
Long Zhou/ 2020 [25]	Yes	Cycle Westerian GAN	The network combines four types of loss functions: adversarial loss, cycle-consistency loss, identity loss and learning loss	Adam	Not mentioned	Not mentioned	Python 3.5, with TensorFlow and Keras	No	NRMSE PSNR SSIM SUVmean bias SUVmax bias	59.5%
Amirhossein Sanaat/ 2020 [26]	Yes	UNET	Mean squared error loss function	Adam optimizer	Not mentioned	Not mentioned	Not mentioned	Yes	PSNR, SSIM, Region-wise SUV bias,	66.6%

Table 3 (continued)

author/ publication date	Preprocessing data	DL method/ configuration					Platform	qualitative evaluations	Image quality metrics (quantitative analysis/ clinical metrics)	CLAIM results (percentage)
		model	loss function	optimizer	Training techniques	Evaluation method				
Karl Spuhler/ 2020 [27]	Not mentioned	Dilated CNN	L1-error	Adam optimizer	Residual learning	Not mentioned	Python 2.7.15, TensorFlow 1.14.0	No	MAPE, PSNR, SSIM	59.5%
Kevin T. Chen/ 2020 [28]	Yes	UNET	Not mentioned	Not mentioned	Transfer learning	fivefold cross-validation	Not mentioned	No	PSNR SSIM RMSE	59.5%
Si Young Yie / 2020 [29]	Not mentioned	Noise2Noise technique with UNET setup	MSE	Adam Optimizer	self-supervised methods	Not mentioned	PyTorch	No	PSNR SSIM	59.5%
Abolfazl Mehranian/ 2020 [30]	Yes	CNN	MSE	Adam	A combination of deep learning and model-based methods	Not mentioned	PyTorch	No	NRMSE	71.4%
Qiupeng Feng/ 2020 [31]	Yes	CNN and GAN	Mean Squared Error (MSE) loss L2 for sinogram module and the perceptual consistency loss for reconstruction module	Adam algorithm	Residual connection	Not mentioned	Not mentioned	No	PSNR SSIM	50%
Yang Lei/ 2020 [32]	Not mentioned	Cycle-GAN	MSE used for generators and binary cross entropy (BCE) for discriminator	Adam gradient descent	Self-attention strategy	four-fold cross-validation	Not mentioned	No	ME NMSE NCC PSNR	45.2%
Amirhossein Sanaat/ 2021 [33]	Yes	Cycle-GAN	Not mentioned	mini-batch size of 6	Not mentioned	independent validation using an external dataset for a single trained model	Tensorflow	Yes	MSE PSNR SSIM region-wise SUV bias STD	80.9%
Bo Zhou / 2021 [34]	Yes	Temporal Siamese Pyramid Network	A combination of registration loss, denoising loss, and adversarial loss	ADAM optimizer	Not mentioned	four-fold cross validation	Pytorch	No	PSNR SSIM NMAE	71.4%

Table 3 (continued)

author/ publication date	Preprocessing data	DL method/ configuration					Platform	qualitative evaluations	Image quality metrics (quantitative analysis/ clinical metrics)	CLAIM results (percentage)
		model	loss function	optimizer	Training techniques	Evaluation method				
Zhanli Hu/ 2021 [35]	Yes	Wasserstein GAN	Combining perceptual loss, mean square error, and the Wasserstein distance as the loss function	Adam optimizer	Not mentioned	Not mentioned	TensorFlow Python library	No	*SSIM* *PSNR*	64.2%
Yan-Ran (Joyce) Wang/ 2021 [36]	Yes	CNN	Attention-weighted loss	ADAM optimizer	Not mentioned	Leave-one-out cross-validation	Not mentioned	Yes	PSNR, SSIM, NRMSE	76.2%
Hui Liu / 2021 [37]	Not mentioned	UNET	L2 loss	Adam optimizer	Not mentioned	Ten extremely obese subjects used as external validation	Not mentioned	Yes	NSTD the ratio of the lesion SUV to lung SUV	61.9%
Hengzhi Xue / 2021 [38]	Yes	Cycle-GAN	Adversarial loss, Cycle consistency loss, Supervised loss	Adam optimizer	Not mentioned	Not mentioned	TensorFlow	No	PSNR MSE	59.5%
Kevin T. Chen/ 2021 [39]	Yes	UNET	L1 norm	Adaptive moment estimation	Not mentioned	Ninefold cross-validation	Not mentioned	Yes	PSNR SSIM RMSE	59.5%
Viswanath P. Sudarshan/ 2021 [40]	Not mentioned	UNET	A loss function that combines image-domain, sinogram-domain, and uncertainty-aware terms	ADAM optimizer	Not mentioned	Not mentioned	Not mentioned	No	PSNR SSIM	61.9%
Song Xue / 2021 [41]	Yes	Conditional GAN	Conventional content loss and voxelwise loss	Not mentioned	Not mentioned	Not mentioned	Not mentioned	Yes	SSIM	73.8%
Ashok J. Theruvath / 2021 [42]	Not mentioned	CNN	Not mentioned	Not mentioned	Not mentioned	Not mentioned	Not mentioned	Yes	SUVmax SUVmean	54.7%
Akshay S. Chaudhari/ 2021 [43]	Not mentioned	CNN	Not mentioned	Not mentioned	Not mentioned	external validation test	Not mentioned	Yes	Not mentioned	52.3%

Table 3 (continued)

author/ publication date	Preprocessing data	DL method/ configuration					Platform	qualitative evaluations	Image quality metrics (quantitative analysis/ clinical metrics)	CLAIM results (percentage)
		model	loss function	optimizer	Training techniques	Evaluation method				
Christian J. Park/ 2021 [44]	Yes	UNET	Mean squared error	Adam optimizer	Not mentioned	Leave-one-out cross validation	Keras with a Tensorflow backend	Yes	SSIM NRMSE PSNR	59.5%
Claes Nøhr Ladefoged / 2021 [45]	Yes	UNET	Huber loss	ADAM	Not mentioned	Six-fold cross-validation	Not mentioned	Yes	PSNR NRMSE	61.9%
Zhao Peng / 2021 [46]	Yes	Wasserstein GAN	The Generator uses a mixed loss function includes Mean Absolute Error and the Wasserstein distance	Adam algorithm	Not mentioned	fivefold cross-validation	Keras with Tensorflow as the backend	Yes	NRMSE SSIM PSNR	61.9%
Ali Ghafari / 2022 [47]	Not mentioned	Cycle-GAN	Mean squared error was used as the adversarial loss function,Mean Absolute error was used for identity and cycle consistency losses as loss functions	ADAM optimizer	Not mentioned	An image data of a patient scanned with 68 Ga-PSMA used as the external validation	Not mentioned	Yes	PSNR SSIM NRMSE SUVmean, SUVmax	66.6%
Yan Xing/ 2022 [48]	Yes	UNET	L1 Loss	ADAM optimizer	Residual learning	80 studies were used for validation (externally)	PyTorch framework and Python 3.7	Yes	SUVmean, SUVmax, SD, liver SNR, TBR, TsBR	66.6%
Yang Zhou / 2022 [49]	Yes	GAN	Adversarial loss and L1 norm as the content loss	Non-momentum-based optimizer RMSprop	Segmentation Guided Strategy	A 21-fold cross-validation and 200 pairs of simulated data for External Validation	Pytorch	No	PSNR, SSIM, MAE	64.2%
Tomoyuki Fujioka / 2022 [50]	Not mentioned	Pix2pix GAN	a combination of two terms: the adversarial loss and the L1 loss	Adam	Not mentioned	Not mentioned	Deep Analyzer; GHELIA,	Yes	PSNR, SSIM	59.5%

Table 3 (continued)

author/ publication date	Preprocessing data	DL method/ configuration					Platform	qualitative evaluations	Image quality metrics (quantitative analysis/ clinical metrics)	CLAIM results (percentage)
		model	loss function	optimizer	Training techniques	Evaluation method				
Bart M. de Vries 2022 [51]	Yes	CNN	Not mentioned	Adam optimizer	Transfer-learning	Not mentioned	Keras library (v2.2) in Python (v3.6), which is based on Tensor-flow (v.1.13.1) as backend	Yes	SSIM PSNR	69%
Hanyu Sun / 2022 [52]	Not mentioned	GAN	a combined loss, includ-ing the mean absolute error, structural loss, and bias loss	Adam optimizer	Not mentioned	Four-fold cross-validation and hold-out valida-tion	TensorFlow 2.2.0	No	PSNR NMSE SSIM CNR	54.7%
Yanmei Luo 2022 [53]	Not mentioned	GAN	Composed of adversarial loss, traditional pixel-level loss and pixel-level estimation error loss	Adam optimizer	Not mentioned	Not mentioned	Pytorch frame-work	No	PSNR SSIM MSE	57%
René Hosch / 2022 [54]	Yes	pix2pixHD GAN	a feature-matching loss	Not mentioned	Not mentioned	Fivefold cross-validation	Not mentioned	Yes	SSIM PSNR MAE SUVmax SUVmean SUVpeak	64.2%
Raphaël Sura Daveau / 2022 [55]	Yes	UNET	mean absolute error	Adam optimizer	Not mentioned	Not mentioned	PyTorch	No	SSIM, PSNR NRMSE COV SUVr	61.9%
Fuquan Deng / 2022 [56]	Yes	discrete-wave-let-transform CNN	Perceptual loss, mean-square-error loss and kernel loss	ADAM opti-mizer	Not mentioned	Not mentioned	Not mentioned	Yes	PSNR NMSE RCNR	69%
Lipei Zhang / 2022 [57]	Yes	Siamese encoder net-work	L1 loss	Adam	Not mentioned	Six-fold cross-validation with 60 patient and 10 patients for external validation	PyTorch 1.6.0 backend	No	RSME SSIM PSNR PCC	66.6%

Table 3 (continued)

author/ publication date	Preprocessing data	DL method/ configuration					Platform	qualitative evaluations	Image quality metrics (quantitative analysis/ clinical metrics)	CLAIM results (percentage)
		model	loss function	optimizer	Training techniques	Evaluation method				
Taisong Wang / 2022 [58]	Yes	CNN	L1 loss	The adaptive moment estimation optimization algorithm	Progressive learning strategy to learn the features of the image data and progressively refine the image quality	Not mentioned	Pytorch 1.5.0	No	SUV tumor-to-liver ratio (TLR) coefcient of variation (COV) in the liver	71.4%
Takaaki Yoshimura / 2022 [59]	Yes	Residual dense network	Not mentioned	Not mentioned	Not mentioned	ninefold cross-validation	Not mentioned	No	PSNR SSIM MSE	61.9%
Rui Hu / 2022 [60]	Not mentioned	Transformer	MSE	Adam optimizer	Not mentioned	Not mentioned	Pytorch 1.7	No	PSNR SSIM MCRC	64.2%
Bo Zhou / 2023 [61]	Not mentioned	UNET	L2 loss	Adam solver	Federated learning, Transfer learning	Not mentioned	Python with Pytorch	No	PSNR SSIM NMSE RMSE	66.6%
Jiadong Zhang / 2023 [62]	Yes	UNET	MSE (measuring voxel-wise errors)	ADAM optimizer	Dynamic convolution	Four-fold cross-validation	PyTorch platform	No	PSNR NRMSE	57%
Caiwen Jiang / 2023 [63]	Yes	Auto-encoder network	A novel structural consistency loss	Adam optimizer	Semi-supervised strategy, introduce region-adaptive normalization and structural consistency constraint to faithfully preserve anatomical structure during the image generation process	Two-fold cross-validation	PyTorch platform	No	NMSE PSNR SSIM	57%
Yuya Onishi / 2023 [64]	Not mentioned	3D encoder-decoder networks	L2 loss	Stochastic gradient descent algorithm	Self-supervised learning	Not mentioned	PyTorch 1.6.0		CNR CNRIR	59.5%

Table 3 (continued)

author/ publication date	Preprocessing data	DL method/ configuration					Platform	qualitative evaluations	Image quality metrics (quantitative analysis/ clinical metrics)	CLAIM results (percentage)
		model	loss function	optimizer	Training techniques	Evaluation method				
Yu Fu / 2023 [65]	Yes	GAN	A combination of adversarial loss, perceptual loss, and structural similarity loss	Adam optimizer	Not mentioned	tenfold cross-validation	PyTorch	Yes	PSNR, SSIM, FSIM, SUVR,	64.2%
Yiyi Hu / 2023 [66]	Yes	UNET	Mean squared error (MSE)	Not mentioned	Not mentioned	Not mentioned	Not mentioned	Yes	SUVmax, SUVmean, SD in the VOI, SNR in the liver, CNR	76.2%
Kun Liu / 2023 [67]	Not mentioned	CNN	Mean square error (MSE)	Adam	Residual learning	Not mentioned	Python2.7and Pytorch0.41	No	PSNR, SSIM,	61.9%
Behnoush Sanaei / 2023 [68]	Not mentioned	ResNet	L2-norm	Adam optimizer	Not mentioned	Five percent of the dataset was considered as the evaluation set within the training process. Among the 140 patient datasets, 40 cases were regarded as the external dataset	NiftyNet platform in Python environment,	No	SSI PSNR RMSE SUVmean bias SUVmax bias	71.4%
Se-In Jang/ 2023 [69]	Not mentioned	Transformer	Charbonnier loss	AdamW optimizer	Not mentioned	Not mentioned	Not mentioned	No	PSNR SSIM CNR	54.7%

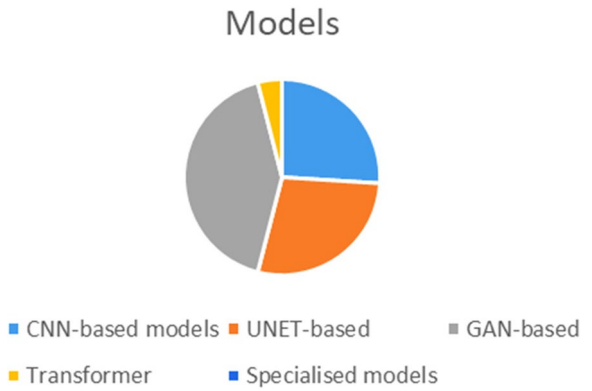

Fig. 2 Models frequency

following an auto-context strategy to iteratively refine the results. A residual CNN was developed by Kaplan et al. [14] in 2019, which integrated specific image features into the loss function to preserve edge, structural, and textural details for successfully eliminating noise from a 1/10th of a FD PET image.

In their work, Gong et al. [21] trained a kind of CNN using simulated data and fine-tuned it with real data to remove noise from PET images of the brain and lungs. In subsequent research, Wang et al. [36] conducted a similar study aimed at enhancing the quality of whole-body PET scans. They achieved this by employing a CNN in conjunction with corresponding MR images. Spuhler et al. [27] employed a variant of CNN with dilated kernels in each convolution, which improved the extraction of features. Mehranian et al. [30] proposed a forward backward splitting algorithm for Poisson likelihood and unrolled the algorithm into a recurrent neural network with several blocks based on CNN.

Researches has also demonstrated the strength of employing a CNN with a UNET structure for the production of high-fidelity PET images. Xu et al. [13] demonstrated in 2017 that a UNET network can be utilized to accurately map the difference between the LD-PET image and the reference FD-PET image by administering only a 1/200th of the injection. Notably, the skip connection of the UNET was specifically utilized to improve the efficient learning of image details. Chen et al. (2019) [17] suggested to combine both LD PET and multiple MRI as conditional inputs for the purpose of producing high quality and precise PET images utilizing a UNET architecture. Cui et al. [22] proposed an unsupervised deep learning method by UNET structure for PET image denoising, where the patient's MR prior image is used as the network input and the noisy PET image is used as the training label. Their method does not require any high-quality images as training labels, nor any prior training or large datasets. In their study, Lu et al. [19] demonstrated that utilizing just 8 LD images of lung cancer patients generated from 10% of the corresponding FD images to train a 3D UNET model resulted in significant noise reduction and reduced bias in the detection of lung nodules. Sanaat et al. (2020) introduced a slightly different approach [26], demonstrating that by using UNET for learning a mapping between the LD-PET sinogram and the FD PET sinogram, it is possible to achieve some improvements in the reconstructed FD PET images. Also, by using UNET structure, Liu et al. [37] were able to reduce the noise of clinical PET images for very obese people to the noise level of thin people. The proposed model by Sudarshan et al. [40] uses UNET that incorporates the physics of the PET imaging system and the heteroscedasticity of the residuals in its loss function, leading to improved robustness to out-of-distribution data. In contrast to previous research that focused on specific body regions, Zhang et al. [62] propose a comprehensive framework for hierarchically reconstructing total-body FD PET images. This framework addresses the diverse shapes and intensity distributions of different body parts. It employs a deep cascaded U-Net as the global total-body network, followed by four local networks to refine the reconstruction for specific regions: head-neck, thorax, abdomen-pelvic, and legs.

On the other hand, more researchers design GAN-like networks for SPET image estimation. GANs have a more complex structure and can solve some problems attributed to CNNs, such as generating blurry results, with their structural loss. For example, Wang et al. [15] (2018) developed a comprehensive framework utilizing 3D conditional GANs with adding skip links to the original UNET network. Further their study in 2019 [20] specifically focused on multimodal GANs and local adaptive fusion techniques to enhance the fusion of multi-modality image information in a more effective manner. Unlike two-dimensional (2D) models, the 3D convolution operation implemented in their framework prevents the emergence of discontinuous cross-like artifacts. According to a study conducted by Ouyang et al. (2019) [18], which employs a GAN architecture with a pretrained amyloid status classifier utilizing feature matching in the discriminator can produce comparable results even in the absence of MR information. Gong et al. implemented a GAN architecture called PT-WGAN [23], which utilizes a Wasserstein Generative Adversarial Network to denoise LD PET images. The PT-WGAN framework uses a parameter transfer strategy to transfer the parameters of a pre-trained WGAN to the PT-WGAN network. This allows the PT-WGAN network to learn from the pre-trained WGAN and improve its performance in denoising LD PET images. Hu et al. [35]in a similar work use

Westerian GAN to directly predict the FD PET image from low-dose PET sinogram data. Xue et al. developed a deep learning method to recover high-quality images from LD PET scans using a conditional GAN model. The model was trained on ^{18}F-FDG images from one scanner and tested on different scanners and tracers. Zhou et al. [49] proposed a novel segmentation guided style-based generative adversarial network for PET synthesis. This approach leverages 3D segmentation to guide the GANs, ensuring that the generated PET images are accurate and realistic. By integrating style-based techniques, the method enhances the quality and consistency of the synthesized images. Fujioka et al. [50] applies the pix2pix GAN to improve the image quality of low-count dedicated breast PET images. This is the first study to use pix2pix GAN for dedicated breast PET image synthesis, which is a challenging task due to the high noise and low resolution of dedicated breast PET images. In a similar work by Hosch et al. [54], the framework of image-to-image translation was used to generate synthetic FD PET images from the ultra-low-count PET images and CT images as inputs and employed group convolution to process them separately in the first layer. Fu et al. [65] introduced an innovative GAN architecture known as AIGAN, designed for efficient and accurate reconstruction of both low dose CT and LD PET images. AIGAN uses a combination of three modules: a cascade generator, a dual-scale discriminator, and a multi-scale spatial fusion module. This method enhances the images in stages, first making rough improvements and then refining them with attention-based techniques.

Recently, there have been articles that highlight the Cycle-GAN model as a variation of the GAN framework. Lei et al., [16] used a Cycle-GAN model to accurately predict FD whole-body ^{18}F-FDG PET images using only 1/8th of the FD inputs. In another study [32], in 2020 they used a similar approach incorporating CT images into the network to aid the process of PET image synthesis from LD on a small dataset consisting of 16 patients. Additionally, in 2020, Zhou et al. [25] proposed a supervised deep learning model rooted in Cycle-GAN for the purpose of PET denoising. Ghafari et al. [47] introduced a Cycle-GAN model to generate standard scan-duration PET images from short scan-duration inputs. The authors evaluated model performance on different radiotracers with different scan durations and body mass indexes. They also report that the optimal scan duration level depends on the trade-off between image quality and scan efficiency.

Some other architecture according to our knowledge by Zhou [61] and et al. proposed a federated transfer learning (FTL) framework for LD PET denoising using heterogeneous LD data. The authors mentioned that their method using a UNET network can efficiently utilize heterogeneous LD data without compromising data privacy for achieving superior LD PET denoising performance for different institutions with different LD settings, as compared to previous FL methods. In a different work, Yie et al. [29] applied the Noise2Noise technique, which is a self-supervised method, to remove PET noise. Feng (2020) et al. [31] presented a study using CNN and GAN for PET sinograms denoising and reconstruction respectively.

The architecture chosen for training can be trained with different configurations and input data types. In the following, we review the types of inputs used in the extracted articles including 2D, 2.5D, 3D, multi-channel and multi-modality. According to our findings, there have been several studies conducted on 2D inputs (single-slice or patch) [12, 14, 17, 21, 24, 25, 27, 29, 47, 50, 52, 53, 56, 57, 67, 68]. In these studies, researchers extracted slices or patches from 3D images and treated them separately for training the model. 2.5 dimensional model (multi-slice) involves stacking adjacent slices for incorporating morphologic information [13, 18, 36, 40, 42–44, 46, 48, 54, 61, 65]. Studies that train models on a 2.5D multi-slice inputs differ from those utilizing a 3D convolution network. The main difference between 2.5D and 3D inputs is the way in which the data is represented. 3D approach employs the depth-wise operation and occurs when the whole volume is considered as input. 16 studies investigated 3D training approach [15, 16, 19, 20, 22, 23, 32, 34, 37, 41, 45, 49, 51, 55, 62, 66]. Multi-channel input refers to input data with multiple channels, where each channel represents a different aspect of the input. By processing each channel separately before combining them later on, the network can learn to capture unique information from each channel that is relevant to the task at hand. Papers [12, 68] used this technique as input to their model, enabling the network to learn more complex relationships between data features. Additionally, some researchers utilized multi-modality data to provide a complete and effective information for their models. For instance, combining structural information obtained from CT [32, 45, 54, 62, 66] and MRI [12, 17, 20, 36, 40, 42, 52, 56, 57] scans with anatomical/functional information from PET images contributes to better image quality.

The choice of loss function is another critical setting in deep neural networks because it directly affects the performance and quality of the model. Different loss functions prioritize different aspects of the predictions, such as accuracy, smoothness, or sparsity. Among the reviewed articles, the Mean Squared Error (MSE) loss function has been chosen the most [12, 26, 29, 32, 44, 60, 62, 66, 67], while the L1 and L2 functions have only been used in eight studies [13, 15, 17, 20, 27, 39, 48, 57, 58] and

five studies [19, 22, 37, 61, 68], respectively. While MSE (as a variant of L2) emphasizes larger errors, The mean absolute error (MAE) loss (as a variant of L1) focuses on the average magnitude of errors by calculating the absolute difference between corresponding pixel values [55]. The Huber loss function combines the benefits of both MSE and MAE by incorporating both squared and absolute differences [45].

The problem of blurry network outputs with the MSE loss function led to the adoption of perceptual loss as a training loss function [21, 31, 56]. This loss function is based on features extracted from a pretrained network, which can better preserve image details compared to the pixel-based MSE loss function. The use of features such as gradient and total variation, with the MSE in the loss function was another method that was used to preserve the edge, structural details, and natural texture [14]. To solve the problems of adversarial learning in relation to hallucinated structures and instability in training as well as synthesizing images of high-visual quality while not matching with clinical interpretations, The optimization loss functions, including pixel-wise L1 loss, structured adversarial loss [49, 50], and task-specific perceptual loss ensure that images generated by the generator closely match the expected value of the features on the intermediate layers of the discriminator [18]. In supervised fashion of Cycle-GANs that LD PET and FD one is paired, four type of losses employed, including adversarial loss, cycle-consistency loss, identity loss, and supervised learning loss [24, 25, 47]. Different combinations of loss functions can be used for different purposes to guide the model to generate images or volumes that are similar to the ground truth data [32, 35, 40, 41, 46, 52, 53, 56, 65].

At the end for validation of models, studies utilized different datasets for validation, including external datasets and cross-validation on the same training dataset.

Evaluation metrics

In order to assess the effectiveness of synthesizing PET images, two methods were employed: quantitative evaluation of image quality and qualitative evaluation of predicted FD images from LD images. Various denoising techniques were utilized to measure image-wise similarity, structural similarity, pixel-wise variability, noise, contrast, colorfulness and signal-to-noise ratio between estimated PET images and their corresponding FDPET images. Studies shows that peak signal to noise ratio (PSNR) was the most popular metrics used for quantitative image evaluation. Other methods include the normalized root mean square error (NRMSE), structural similarity index metrics (SSIM), Normalized mean square error (NMSE), root mean square error (RMSE), Frequency-based blurring measurement (FBM), edge-based blurring measurement (EBM), contrast recovery coefficient (CRC), contrast-to-noise ratio (CNR), signal to noise ratio (SNR). Additionally, mean and maximum standard uptake value (SUV_{mean} and SUV_{max}) bias were obtained for clinical semi-quantitative evaluation. Several studies have used physician evaluations to clinically assess PET images generated by different models, along with corresponding reference FD and LD PET images.

Discussion

The objective of the reviewed articles is to estimate high-quality, FD PET images from LD PET images by deep learning. This is a challenging problem because the LD PET images have reduced signal-to-noise ratio (SNR) and contrast compared to the FD images. To address this issue, researchers have proposed various models such as CNNs and GANs with varying structures to generate high-quality images from low-quality inputs.

Despite the potential of deep learning-based techniques for estimating FD PET images from LD scans, several challenges still exist to investigated studies. First, the LD data used were randomly under-sampled from the FD PET, instead of using data with true injected LD. Researchers should be further evaluating their models with the actual ultra-low-dose acquisition.

The next challenge to studies is not evaluating the clinical impact or utility of the proposed method, such as its effect on diagnosis, prognosis, or treatment planning, which are important outcomes for PET imaging applications. Deep learning models can produce estimated FD PET images that are quantitatively similar to true FD images, this does not necessarily mean they have equivalent clinical utility and actionability. Thus, rigorous clinical validation studies involving real patients and clinicians are essential before these techniques can be adopted in medical practice. However, most studies evaluated performance using only image-based metrics, without assessing the impact on actual clinical tasks and outcomes.

Another challenge faced by most of the investigated researches, as is usually the case for medical imaging, is the limited number of training data from a single PET system, which may limit the generalizability and robustness of the proposed method to different scanners, protocols, and populations for which measures such as data augmentation methods, cross-validation, slicing and patch-based training, and 2D inputs were explained.

The 2D input of models is often due to the limited amount of training data available and the complexity of the task still presents challenges to research. This can lead to the discontinuous cross-slice estimation issue where the model produces inconsistent or unrealistic results across adjacent slices in the reconstructed image.

To mitigate this issue, some researchers have proposed alternative approaches such as 3D GANs or incorporating additional information such as multi-modal imaging data into the model. These methods can help improve the consistency and quality of the reconstructed images.

Another challenge is the limited choice of loss functions used in these models, which can impact the performance and characteristics of the synthesized FD images. Many studies used L1 or MSE losses that do not fully preserve edge and texture details in the synthesized images. Loss functions that incorporated perceptual losses or emphasized edge and texture preservation produced higher-quality images with less blurring and artifacts. Multi-component losses that combined adversarial, perceptual and pixel-wise losses were found to be effective in some CNNs.

LD PET acquisitions offer several clinical benefits. They can detect lesions and assess tumors while cutting radiation exposure, crucial for pediatric cases and frequent scans. Faster LD scans boost clinic throughput, lower costs, and extend PET access. Combining LD PET with MRI or CT unlocks advanced imaging. Deep learning personalizes PET doses for each patient. This innovative approach promises safer, more efficient, and accessible PET imaging. Clinical studies are pending to confirm its effectiveness. Future validation could lead to new clinical standards.

Conclusions

In conclusion, while deep learning-based approaches show early success in synthesizing Full-Dose PET images from Low-Dose scans, further technical advances, larger datasets, improved model evaluation and extensive clinical validation are still required before these techniques can be reliably adopted in clinical practice.

Abbreviations

PET/CT	Positron Emission Tomography / Computed Tomography
FDG	^{18}F-2-fluoro-2-deoxy-D-glucose
SUV	Standardized Uptake Value
SNR	Signal to Noise Ratio
CNR	Contrast to Noise Ratio
FWHM	Full Width at Half Maximum
CR	Contrast Recovery
LD	Low-Dose
FD	Full-Dose

Supplementary Information

The online version contains supplementary material available at https://doi.org/10.1186/s12880-024-01417-y.

Supplementary Material 1.

Acknowledgements

We acknowledge the contribution of artificial intelligence in improving the grammatical precision and overall writing excellence of this article.

Authors' contributions

NG.S. and P.S. conceived the research idea and developed the research methodology. NG.S.,A.G, N.S and P.S authored the main manuscript. All authors analyzed and validated the data and reviewed the manuscript.

Funding

This study is supported by a grant received from the Iran University of Medial Science by number of 24177.

Availability of data and materials

All data generated or analysed during this study are included in this published article.

Declarations

Ethics approval and consent to participate

This research project has been conducted in accordance with the ethical code IR.IUMS.REC.1401.712.

Consent for publication

Not applicable.

Competing interests

The authors declare no competing interests.

Received: 7 March 2024 Accepted: 30 August 2024
Published online: 11 September 2024

References

1. Gillings N. Radiotracers for positron emission tomography imaging. Magn Reson Mater Phys, Biol Med. 2013;26:149–58.
2. Boellaard R. Standards for PET image acquisition and quantitative data analysis. J Nucl Med. 2009;50(Suppl 1):11S–20S.
3. Arabi H, Zaidi H. Improvement of image quality in PET using post-reconstruction hybrid spatial-frequency domain filtering. Phys Med Biol. 2018;63(21):215010.
4. Wallach, D., Lamare, F., Roux, C. and Visvikis, D., 2010, October. Comparison between reconstruction-incorporated super-resolution and super-resolution as a post-processing step for motion correction in PET. In IEEE Nuclear Science Symposuim & Medical Imaging Conference (pp. 2294–2297). IEEE..
5. Fin L, Bailly P, Daouk J, Meyer ME. A practical way to improve contrast-to-noise ratio and quantitation for statistical-based iterative reconstruction in whole-body PET imaging. Med Phys. 2009;36(7):3072–9.
6. Li Y. Noise propagation for iterative penalized-likelihood image reconstruction based on Fisher information. Phys Med Biol. 2011;56(4):1083.
7. Yu, S. and Muhammed, H.H., 2016, October. Comparison of pre-and post-reconstruction denoising approaches in positron emission tomography. In 2016 1st International Conference on Biomedical Engineering (IBIOMED) (pp. 1–6). IEEE..
8. Riddell C, Carson RE, Carrasquillo JA, Libutti SK, Danforth DN, Whatley M, Bacharach SL. Noise reduction in oncology FDG PET images by iterative reconstruction: a quantitative assessment. J Nucl Med. 2001;42(9):1316–23.
9. Akamatsu G, Ishikawa K, Mitsumoto K, Taniguchi T, Ohya N, Baba S, Abe K, Sasaki M. Improvement in PET/CT image quality with a combination of point-spread function and time-of-flight in relation to reconstruction parameters. J Nucl Med. 2012;53(11):1716–22.
10. Moher D, et al. Preferred reporting items for systematic reviews and meta-analyses: the PRISMA statement. Ann Intern Med. 2009;151(4):264–9.
11. Mongan J, Moy L, Kahn CE Jr. Checklist for artificial intelligence in medical imaging (CLAIM): a guide for authors and reviewers. Radiol Artif Intell. 2020;2(2):e200029.
12. Xiang L, et al. Deep auto-context convolutional neural networks for standard-dose PET image estimation from low-dose PET/MRI. Neurocomputing. 2017;267:406–16.

13. Xu, J., et al., 200x low-dose PET reconstruction using deep learning. arXiv preprint arXiv:1712.04119, 2017.
14. Kaplan S, Zhu Y-M. Full-dose PET image estimation from low-dose PET image using deep learning: a pilot study. J Digit Imaging. 2019;32(5):773–8.
15. Wang Y, et al. 3D conditional generative adversarial networks for high-quality PET image estimation at low dose. Neuroimage. 2018;174:550–62.
16. Lei Y, et al. Whole-body PET estimation from low count statistics using cycle-consistent generative adversarial networks. Phys Med Biol. 2019;64(21):215017.
17. Chen KT, et al. Ultra–low-dose 18F-florbetaben amyloid PET imaging using deep learning with multi-contrast MRI inputs. Radiology. 2019;290(3):649–56.
18. Ouyang J, et al. Ultra-low-dose PET reconstruction using generative adversarial network with feature matching and task-specific perceptual loss. Med Phys. 2019;46(8):3555–64.
19. Lu W, et al. An investigation of quantitative accuracy for deep learning based denoising in oncological PET. Phys Med Biol. 2019;64(16):165019.
20. Wang Y, et al. 3D auto-context-based locality adaptive multi-modality GANs for PET synthesis. IEEE Trans Med Imaging. 2018;38(6):1328–39.
21. Gong K, et al. PET image denoising using a deep neural network through fine tuning. IEEE Transactions on Radiation and Plasma Medical Sciences. 2018;3(2):153–61.
22. Cui J, et al. PET image denoising using unsupervised deep learning. Eur J Nucl Med Mol Imaging. 2019;46:2780–9.
23. Gong Y, et al. Parameter-transferred Wasserstein generative adversarial network (PT-WGAN) for low-dose PET image denoising. IEEE transactions on radiation and plasma medical sciences. 2020;5(2):213–23.
24. Zhao K, et al. Study of low-dose PET image recovery using supervised learning with CycleGAN. PLoS ONE. 2020;15(9):e0238455.
25. Zhou L, et al. Supervised learning with cyclegan for low-dose FDG PET image denoising. Med Image Anal. 2020;65:101770.
26. Sanaat A, et al. Projection space implementation of deep learning–guided low-dose brain PET imaging improves performance over implementation in image space. J Nucl Med. 2020;61(9):1388–96.
27. Spuhler K, et al. Full-count PET recovery from low-count image using a dilated convolutional neural network. Med Phys. 2020;47(10):4928–38.
28. Chen KT, et al. Generalization of deep learning models for ultra-low-count amyloid PET/MRI using transfer learning. Eur J Nucl Med Mol Imaging. 2020;47:2998–3007.
29. Yie SY, et al. Self-supervised PET denoising. Nucl Med Mol Imaging. 2020;54:299–304.
30. Mehranian A, Reader AJ. Model-based deep learning PET image reconstruction using forward–backward splitting expectation–maximization. IEEE transactions on radiation and plasma medical sciences. 2020;5(1):54–64.
31. Feng, Q. and H. Liu. Rethinking PET image reconstruction: ultra-low-dose, sinogram and deep learning. in Medical Image Computing and Computer Assisted Intervention–MICCAI 2020: 23rd International Conference, Lima, Peru, October 4–8, 2020, Proceedings, Part VII 23. 2020. Springer.
32. Lei, Y., et al. Low dose PET imaging with CT-aided cycle-consistent adversarial networks. in Medical Imaging 2020: Physics of Medical Imaging. 2020. SPIE.
33. Sanaat A, et al. Deep learning-assisted ultra-fast/low-dose whole-body PET/CT imaging. Eur J Nucl Med Mol Imaging. 2021;48:2405–15.
34. Zhou B, et al. MDPET: a unified motion correction and denoising adversarial network for low-dose gated PET. IEEE Trans Med Imaging. 2021;40(11):3154–64.
35. Hu Z, et al. DPIR-Net: Direct PET image reconstruction based on the Wasserstein generative adversarial network. IEEE Transactions on Radiation and Plasma Medical Sciences. 2020;5(1):35–43.
36. Wang Y-R, et al. Artificial intelligence enables whole-body positron emission tomography scans with minimal radiation exposure. Eur J Nucl Med Mol Imaging. 2021;48:2771–81.
37. Liu H, et al. PET image denoising using a deep-learning method for extremely obese patients. IEEE Transactions on Radiation and Plasma Medical Sciences. 2021;6(7):766–70.
38. Xue H, et al. LCPR-Net: low-count PET image reconstruction using the domain transform and cycle-consistent generative adversarial networks. Quant Imaging Med Surg. 2021;11(2):749.
39. Chen KT, et al. True ultra-low-dose amyloid PET/MRI enhanced with deep learning for clinical interpretation. Eur J Nucl Med Mol Imaging. 2021;48:2416–25.
40. Sudarshan VP, et al. Towards lower-dose pet using physics-based uncertainty-aware multimodal learning with robustness to out-of-distribution data. Med Image Anal. 2021;73:102187.
41. Xue, S., et al., A cross-scanner and cross-tracer deep learning method for the recovery of standard-dose imaging quality from low-dose PET. European journal of nuclear medicine and molecular imaging, 2021: p. 1–14.
42. Theruvath AJ, et al. Validation of deep learning–based augmentation for reduced 18F-FDG dose for PET/MRI in children and young adults with lymphoma. Radiol Artif Intell. 2021;3(6):e200232.
43. Chaudhari AS, et al. Low-count whole-body PET with deep learning in a multicenter and externally validated study. NPJ digital medicine. 2021;4(1):127.
44. Park CJ, et al. Initial experience with low-dose 18F-fluorodeoxyglucose positron emission tomography/magnetic resonance imaging with deep learning enhancement. J Comput Assist Tomogr. 2021;45(4):637.
45. Ladefoged CN, et al. Low-dose PET image noise reduction using deep learning: application to cardiac viability FDG imaging in patients with ischemic heart disease. Phys Med Biol. 2021;66(5):054003.
46. Peng Z, et al. Feasibility evaluation of PET scan-time reduction for diagnosing amyloid-β levels in Alzheimer's disease patients using a deep-learning-based denoising algorithm. Comput Biol Med. 2021;138:104919.
47. Ghafari A, et al. Generation of 18F-FDG PET standard scan images from short scans using cycle-consistent generative adversarial network. Phys Med Biol. 2022;67(21):215005.
48. Xing Y, et al. Deep learning-assisted PET imaging achieves fast scan/low-dose examination. EJNMMI physics. 2022;9(1):1–17.
49. Zhou Y, et al. 3D segmentation guided style-based generative adversarial networks for pet synthesis. IEEE Trans Med Imaging. 2022;41(8):2092–104.
50. Fujioka T, et al. Proposal to Improve the Image Quality of Short-Acquisition Time-Dedicated Breast Positron Emission Tomography Using the Pix2pix Generative Adversarial Network. Diagnostics. 2022;12(12):3114.
51. de Vries BM, et al. 3D Convolutional Neural Network-Based Denoising of Low-Count Whole-Body 18F-Fluorodeoxyglucose and 89Zr-Rituximab PET Scans. Diagnostics. 2022;12(3):596.
52. Sun H, et al. High-quality PET image synthesis from ultra-low-dose PET/MRI using bi-task deep learning. Quant Imaging Med Surg. 2022;12(12):5326.
53. Luo Y, et al. Adaptive rectification based adversarial network with spectrum constraint for high-quality PET image synthesis. Med Image Anal. 2022;77:102335.
54. Hosch R, et al. Artificial intelligence guided enhancement of digital PET: scans as fast as CT? Eur J Nucl Med Mol Imaging. 2022;49(13):4503–15.
55. Daveau RS, et al. Deep learning based low-activity PET reconstruction of [11C] PiB and [18F] FE-PE2I in neurodegenerative disorders. Neuroimage. 2022;259:119412.
56. Deng F, et al. Low-Dose 68 Ga-PSMA Prostate PET/MRI Imaging Using Deep Learning Based on MRI Priors. Front Oncol. 2022;11:818329.
57. Zhang L, et al. Spatial adaptive and transformer fusion network (STFNet) for low-count PET blind denoising with MRI. Med Phys. 2022;49(1):343–56.
58. Wang T, et al. Deep progressive learning achieves whole-body low-dose 18F-FDG PET imaging. EJNMMI physics. 2022;9(1):82.
59. Yoshimura T, et al. Medical radiation exposure reduction in PET via super-resolution deep learning model. Diagnostics. 2022;12(4):872.
60. Hu, R. and H. Liu. TransEM: Residual swin-transformer based regularized PET image reconstruction. in International Conference on Medical Image Computing and Computer-Assisted Intervention. 2022. Springer.
61. Zhou B, et al. Federated transfer learning for low-dose pet denoising: a pilot study with simulated heterogeneous data. IEEE Transactions on Radiation and Plasma Medical Sciences. 2022;7(3):284–95.
62. Zhang, J., et al., Hierarchical Organ-Aware Total-Body Standard-Dose PET Reconstruction From Low-Dose PET and CT Images. IEEE Transactions on Neural Networks and Learning Systems, 2023.
63. Jiang, C., et al., Semi-supervised Standard-dose PET Image Generation via Region-adaptive Normalization and Structural Consistency Constraint. IEEE Transactions on Medical Imaging, 2023.

64. Onishi, Y., et al., Self-Supervised Pre-Training for Deep Image Prior-Based Robust PET Image Denoising. IEEE Transactions on Radiation and Plasma Medical Sciences, 2023.
65. Fu Y, et al. AIGAN: Attention–encoding Integrated Generative Adversarial Network for the reconstruction of low-dose CT and low-dose PET images. Med Image Anal. 2023;86:102787.
66. Hu Y, et al. Comparative study of the quantitative accuracy of oncological PET imaging based on deep learning methods. Quant Imaging Med Surg. 2023;13(6):3760.
67. Liu K, et al. A Lightweight Low-dose PET Image Super-resolution Reconstruction Method based on Convolutional Neural Network. Current Medical Imaging. 2023;19(12):1427–35.
68. Sanaei, B., R. Faghihi, and H. Arabi, Employing Multiple Low-Dose PET Images (at Different Dose Levels) as Prior Knowledge to Predict Standard-Dose PET Images. J Digit Imaging, 2023: p. 1–9.
69. Jang, S.-I., et al., Spach Transformer: Spatial and channel-wise transformer based on local and global self-attentions for PET image denoising. IEEE transactions on medical imaging, 2023.

Publisher's Note